Instability of a fluctuating membrane driven by an ac electric field

Jacopo Seiwert[1] and Petia M. Vlahovska[2]
[1]*Institut de Physique de Rennes UMR 6251, Université de Rennes, 35042 Rennes, France*
[2]*School of Engineering, Brown University, Providence, Rhode Island 02912, USA*
(Received 2 July 2012; revised manuscript received 4 December 2012; published 19 February 2013)

Shape fluctuations of a planar lipid membrane in an ac electric field are investigated using a zero-thickness electromechanical model, which accounts for membrane conductivity and capacitance, and asymmetry in the properties of the fluids separated by the membrane. A linear stability analysis shows that unlike in the case of a dc electric field, a purely capacitive membrane can be destabilized in an ac electric field. The theory highlights that the instability originates from electric pressure exerted on the membrane.

DOI: 10.1103/PhysRevE.87.022713 PACS number(s): 87.16.dj, 47.65.−d, 47.15.G−

I. INTRODUCTION

Living cells maintain an electric potential difference across their plasma membranes. Changes in the transmembrane electric field are biologically important signals in physiological processes such as signal propagation in neurons via action potentials [1,2] and electric-field-directed cell migration [3,4] in development and regeneration [5,6].

The transmembrane potential can be modulated intrinsically through transport of ions between the extracellular and intracellular spaces or ionization of membrane lipids (e.g., due to changes in *p*H), or externally through application of electric fields. Intrinsically charged membranes have been theoretically studied in order to predict the renormalization of the bending rigidity and tension [7–12], membrane fluctuations, and stability [13–17]. Similar studies of membranes in externally applied electric fields have only recently appeared [18–25] (reviewed in [26,27]). Progress has been slow because of the nonequilibrium nature of the problem, which involves coupled evolution of electric fields, membrane shape, and flow in the surrounding fluids. As a result, much of the rich dynamics displayed by lipid membranes in electric fields [28,29] remains unexplained. For example, in dc fields quasispherical vesicles can deform into spherocylinders [30], burst [31], or porate [32,33]. ac fields drive frequency-dependent membrane flows [34] and membrane destabilization [35]. ac fields are widely used in vesicle electroformation; hence understanding of ac-field-driven instabilities may shed light on the vesicle formation mechanism. All theoretical analyses of membrane stability so far have focused on dc fields and established several destabilizing mechanisms: electric-field-induced negative surface tension [18], electrokinetic flows [19], and electric pressure and shear stress in the case of a membrane separating solutions with different conductivities [24,25]. In real systems, these different sources of instability are most likely all operational, but one may dominate depending on the parameters of the experiment. For example, when the membrane is surrounded by fluids of the same conductivity, only the first two effects are relevant. In this paper, we investigate the possibility of destabilization of a nonconducting membrane, such as the typical lipid bilayer, by the electric pressure generated by an ac field.

II. PROBLEM FORMULATION

Let us consider a planar membrane formed by a charge-free lipid bilayer with dielectric constant ε_m and conductivity σ_m. The molecularly thin bilayer (thickness $d \sim 5$ nm) is treated as a two-dimensional interface with effective capacitance $C_m = \varepsilon_m/d$ and conductance $G_m = \sigma_m/d$. The membrane separates solutions with different viscosities, conductivities, and dielectric constants; see Fig. 1. Far from the membrane a uniform electric field is created by applying a potential V between two electrodes, placed at a distance L on either side. To be able to study both dc and ac situations in the same framework, we consider

$$V(t) = V_0(\sqrt{1-\delta^2}+\delta\sqrt{2}\cos \nu t), \tag{1}$$

where ν is the angular frequency of the field, and δ is a parameter varying between 0 and 1: $\delta = 0$ and $\delta = 1$ correspond to a constant and a purely sinusoidal voltage, respectively. The above expression is chosen because it conserves the root mean square of the potential as the parameter δ is varied (in contrast to the form adopted by Roberts and Kumar [36]).

A. Physical motivation

Let us first recall the response of an insulating planar membrane, $G_m = 0$, subjected to a step electric field with magnitude $E_0 = V_0/2L$ [$E(t<0) = 0$, $E(t>0) = E_0$]. Upon application of the electric field, free charges brought by conduction pile up at the membrane physical surfaces and the membrane acts as a perfect capacitor.

At steady state, the entire voltage drop occurs within the membrane (the transmembrane potential is $V_m = V_0$). The membrane capacitor prevents any electrical current from flowing through the system. Thus, electric fields in the upper and lower solutions vanish and so does the electric pressure on the membrane. Accordingly, the membrane is linearly stable [24,25]. This is in contrast with ordinary fluid-fluid interfaces (e.g., air/water) where the potential is always continuous: bulk electric fields are nonzero and the corresponding electric stresses may act to destabilize the interface [37–39].

However, while the capacitor is charging electric current does flow through the system, and transient electric fields exist in the bulk. The transmembrane potential evolves exponentially in time [24]

$$V_m(t) = V_0(1-e^{-t/t_{m,0}}), \tag{2}$$

where

$$t_{m,0} = LC_m\left(\sigma_2^{-1}+\sigma_1^{-1}\right) \tag{3}$$

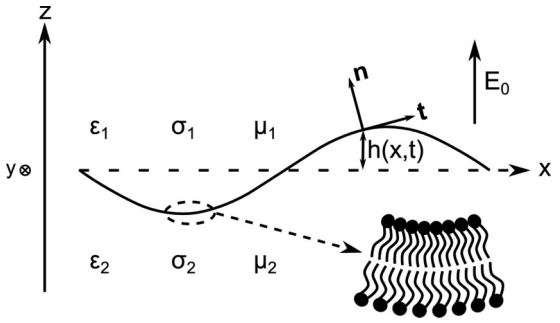

FIG. 1. A freely floating planar lipid bilayer membrane separating fluids with different physical (viscosity μ) and electrical (permittivity ε and conductivity σ) properties. A uniform electric field E_0 is applied far from the membrane. The time-dependent displacement of the membrane above the x-y plane along the z direction is $h(x,y,t)$.

is the capacitor charging time. Hence, we expect that the membrane could become destabilized during this time; this case has been observed in dc electric fields [24]. In this work, we hypothesize that an ac electric field with a period of oscillations comparable to the charging time (3) could maintain electric currents through the membrane, and thus promote membrane instability.

B. Governing equations

Membrane instability involves deformation; interface shape in an electric field is determined by the balance of electric $\boldsymbol{\tau}_{\rm el}$, hydrodynamic $\boldsymbol{\tau}_{\rm hd}$, membrane bending $\boldsymbol{\tau}_{\kappa}$, and tension $\boldsymbol{\tau}_{\Sigma}$ stresses

$$\boldsymbol{\tau}_{\rm el} + \boldsymbol{\tau}_{\rm hd} = \boldsymbol{\tau}_{\kappa} + \boldsymbol{\tau}_{\Sigma}\,. \tag{4}$$

Next we discuss the calculation of these stresses.

1. Membrane mechanics

Elastic properties of lipid membranes are described by the model proposed by Helfrich [40], in which the deformation energy for bending depends quadratically on the departure of the local mean curvature H from its preferred value. The bending tractions derived from the Helfrich energy are [41]

$$\boldsymbol{\tau}_{\kappa} = -\kappa\big[4(H^3 - K_G H) + 2\nabla_s^2 H\big]\mathbf{n}, \tag{5}$$

where κ is the bending modulus, K_G is the gaussian curvature, and ∇_s^2 is the Laplace-Beltrami operator.

Lipid molecules are free to move within a monolayer, and their number in the bilayer is fixed. Accordingly, the membrane can be treated as an incompressible two-dimensional fluid. The membrane tension Σ is a two-dimensional analog of the pressure in incompressible fluids; it is introduced the enforce the constant surface area [42]. The surface force associated with membrane tension has both normal (pressure) and tangential (shear) components,

$$\boldsymbol{\tau}_{\Sigma} = 2\Sigma H\mathbf{n} - \nabla_s\Sigma, \tag{6}$$

where $\nabla_s = \mathbf{I}_s\cdot\nabla$ is the surface gradient operator and $\mathbf{I}_s = \mathbf{I} - \mathbf{nn}$ is the surface projection.

2. Electric field

We adopt the leaky dielectric model, which combines the Stokes equations to describe fluid motion with conservation of current described by Ohm's law, $\mathbf{J} = \sigma\mathbf{E}$ [43]. Even though the model was originally developed for fluids with very low conductivity, it has been shown that it is an exact lumped parameter description in the case of drop electrohydrodynamics [44] and it has been successfully applied to model vesicle electrohydrodynamics [45,46]. The charge of the diffuse layers is effectively included in the induced surface charge density,

$$Q = \mathbf{n}\cdot(\varepsilon_1\mathbf{E}_1 - \varepsilon_2\mathbf{E}_2), \quad z = h. \tag{7}$$

The absence of spatial charge means that the bulk fluids are electroneutral and that the electric field is irrotational, $\mathbf{E} = -\nabla\phi$. Due to the membrane capacitance the potential is discontinuous at the interface $z = h(x,y,t)$, and we define the transmembrane potential as $V_m = \phi_2 - \phi_1$. The current conservation at the top ($z = h^+$) and bottom ($z = h^-$) membrane surfaces is

$$\begin{aligned}\mathbf{n}\cdot(\mathbf{J}_1 - \mathbf{J}_m) &= -\frac{\partial Q_1}{\partial t} - \nabla_s\cdot(\mathbf{v}_s Q_1), \quad z = h^+,\\ \mathbf{n}\cdot(\mathbf{J}_m - \mathbf{J}_2) &= -\frac{\partial Q_2}{\partial t} - \nabla_s\cdot(\mathbf{v}_s Q_2), \quad z = h^-,\end{aligned} \tag{8}$$

where $\mathbf{J}_m$ is the Ohmic current flowing through the membrane (if the membrane is conducting $\mathbf{J}_m = \sigma_m\mathbf{E}_m$). $\mathbf{v}_s$ is the interface velocity; $\mathbf{v}_s Q$ is the convective charge flux along the interface. The charge densities Q_1 and Q_2 on the two surfaces of the membrane facing fluids 1 and 2 are

$$Q_1 = \mathbf{n}\cdot(\varepsilon_1\mathbf{E}_1) - C_m V_m, \quad Q_2 = C_m V_m - \mathbf{n}\cdot(\varepsilon_2\mathbf{E}_2), \tag{9}$$

where for a thin membrane we use the approximation $\varepsilon_m\mathbf{n}\cdot\mathbf{E}_m = C_m V_m$. Note that the apparent induced charge of the membrane (7) is $Q = Q_1 + Q_2$.

If charge convection is negligible then Eqs. (8) and (9) can be rewritten as

$$\begin{aligned}\mathbf{n}\cdot\left(\sigma_2\mathbf{E}_2 + \varepsilon_2\frac{\partial\mathbf{E}_2}{\partial t}\right) &= \mathbf{n}\cdot\left(\sigma_1\mathbf{E}_1 + \varepsilon_1\frac{\partial\mathbf{E}_1}{\partial t}\right),\\ \mathbf{n}\cdot\left(\sigma_2\mathbf{E}_2 + \varepsilon_2\frac{\partial\mathbf{E}_2}{\partial t}\right) &= C_m\frac{\partial V_m}{\partial t} + G_m V_m.\end{aligned} \tag{10}$$

The above equations express the conservation of normal currents through the system. The membrane current has a part due to the charging of the capacitor ($C_m\partial V_m/\partial t$) and an Ohmic part due to membrane conductivity ($G_m V_m$, e.g., arising from pores or channels). Likewise, the current in each fluid is the sum of an Ohmic part $\sigma\mathbf{E}$, and a displacement current $\varepsilon\partial\mathbf{E}/\partial t$ associated with charge relaxation.

The electric force density $\boldsymbol{\tau}_{\rm el}$ acting on the membrane is calculated from the Maxwell tensor,

$$\boldsymbol{\tau}_{\rm el} = \mathbf{n}\cdot\left(\mathbf{T}_1^{\rm el} - \mathbf{T}_2^{\rm el}\right), \quad \mathbf{T}^{\rm el} = \varepsilon\left(\mathbf{EE} - \frac{\mathbf{E}^2}{2}\mathbf{I}\right). \tag{11}$$

The interfacial electric stress has normal (pressure) and tangential (shear) parts,

$$\begin{aligned}p^{\rm el} &\equiv \tau_{{\rm el},n} = \tfrac{1}{2}\big[\varepsilon_1\big(E_{1,n}^2 - E_{1,t}^2\big) - \varepsilon_2\big(E_{2,n}^2 - E_{2,t}^2\big)\big],\\ \tau_{{\rm el},t} &= \varepsilon_1(E_{1,n}E_{1,t}) - \varepsilon_2(E_{2,n}E_{2,t}).\end{aligned} \tag{12}$$

3. Fluid motion

At the length scale of biological membranes, inertia is negligible and the velocity $\mathbf{v}$ and pressure p fields are solutions of the Stokes equation:

$$\mu\nabla^2\mathbf{v} = \nabla p, \quad \nabla\cdot\mathbf{v} = 0. \tag{13}$$

The no-slip boundary condition applies for the velocity at the electrodes, $\mathbf{v}_1(z=L) = \mathbf{v}_2(z=-L) = 0$. Membrane deformation is determined from the kinematic condition that the interface moves with the normal component of the fluid velocity. For a planar membrane,

$$\frac{\partial h}{\partial t} = \mathbf{v}_s\cdot(\hat{\mathbf{z}} - \nabla h), \tag{14}$$

where $\mathbf{v}_1(z=h) = \mathbf{v}_2(z=h) \equiv \mathbf{v}_s$. The area incompressibility of the membrane imposes an additional constraint on the velocity field, $\nabla_s\cdot\mathbf{v}_s = 0$. The viscous forces exerted on the membrane are inferred from the hydrodynamic stress tensor,

$$\boldsymbol{\tau}_{\rm hd} = \mathbf{n}\cdot\left(\mathbf{T}_1^{\rm hd} - \mathbf{T}_2^{\rm hd}\right), \quad \mathbf{T}^{\rm hd} = -p\mathbf{I} + \mu[\nabla\mathbf{v} + (\nabla\mathbf{v})^\dagger], \tag{15}$$

where the dagger denotes the transpose.

C. Dimensionless parameters and rescaling

Upon application of an electric field, bulk fluids become electroneutral on the charge relaxation time scales [47]

$$t_1 = \frac{\varepsilon_1}{\sigma_1}, \quad t_2 = \frac{\varepsilon_2}{\sigma_2}, \tag{16}$$

and the leaky membrane capacitor charges on a time scale (see Appendix A for the derivation)

$$t_m = \frac{LC_m}{\sigma_1}\frac{1+R}{R+g_m(1+R)}, \tag{17}$$

where $g_m = G_mL/\sigma_1$ is the nondimensional membrane conductance and $R = \sigma_2/\sigma_1$. The electric stresses drive membrane deformation accompanied by fluid motion with a time scale

$$t_{\rm el} = \frac{\mu_1+\mu_2}{\varepsilon_1 E_0^2}, \tag{18}$$

where $E_0 = V_0/2L$ is the characteristic magnitude of the imposed electric field. Resistance to changes in membrane curvature drives relaxation on a time scale

$$t_\kappa = \frac{\mu_1+\mu_2}{\kappa q^3}, \tag{19}$$

for a membrane undulation with wave number q.

Henceforth, all quantities are rescaled by the properties of the top fluid. The distance L between the membrane and the electrode is used to rescale all lengths, and it is chosen for two reasons. First, it is the only physical scale of our problem (since we assume the membrane to be infinitely thin and large). Second, it is a crucial experimental parameter determining, for example, the strength of the electric field, for a given potential. Additionally, the charge scale is ε_1E_0, and stresses are scaled by $\varepsilon_1E_0^2$. The systematic analysis of the problem involves four dimensionless parameters:

$$\begin{aligned}\omega &= \nu t_m, \quad {\rm Ca} = \frac{\epsilon_1E_0^2L^3}{\kappa} = \frac{t_\kappa}{t_{\rm el}},\\ \alpha &= \frac{\epsilon_1}{LC_m} \approx \frac{t_1}{t_m}, \quad \beta = \frac{\epsilon_1E_0^2C_mL}{\mu_1\sigma_1} \approx \frac{t_m}{t_{\rm el}}.\end{aligned} \tag{20}$$

α reflects the importance of bulk charge relaxation; β and the capillary number Ca respectively compare viscous and elastic effects to electrical pressure. In addition, the physical properties of the system are characterized by $R = \sigma_2/\sigma_1$ and $S = \varepsilon_2/\varepsilon_1$, which measure the electrical mismatch between the two fluids, the viscosity ratio $\lambda = \mu_2/\mu_1$, and the nondimensional membrane conductance g_m. We also introduce $\xi = \Sigma L^2/\kappa$, which compares the membrane tension to bending forces.

III. PROBLEM SOLUTION

Here we perform a linear stability analysis by studying the dynamics of a shape fluctuation mode $h(x,t) = h_q(t)e^{iqx}$. Without loss of generality we consider only a wave vector parallel to the x axis. Accordingly, any variable u is expanded in a series of the form $u = u^{(0)}(z,t) + u^{(1)}(z,x,t) + \cdots$. The superscript (0) corresponds to the base state, $h = 0$. $u^{(1)} = u_q(z,t)\exp(iqx)$ is a linear correction accounting for the effect of the small undulations. In the next sections, we derive the evolution equations for the amplitudes $u_q(z,t)$ and study their growth rate using Floquet analysis.

A. Base state

In the base state the membrane is flat and fixed at $z = 0$ ($h = 0$). After an initial transient corresponding to the charging of the membrane, the electric fields are spatially homogeneous in each region and may be written as

$$\begin{aligned}E_1^{(0)} &= E_{1,{\rm dc}}^{(0)} + E_{1,c}^{(0)}\cos\omega t + E_{1,s}^{(0)}\sin\omega t,\\ E_2^{(0)} &= E_{2,{\rm dc}}^{(0)} + E_{2,c}^{(0)}\cos\omega t + E_{2,s}^{(0)}\sin\omega t.\end{aligned} \tag{21}$$

The dc components of the fields are

$$E_{2,{\rm dc}}^{(0)} = \frac{g_m\sqrt{1-\delta^2}}{R+g_m(1+R)}, \quad E_{1,{\rm dc}}^{(0)} = RE_{2,{\rm dc}}^{(0)}. \tag{22}$$

As already noted, in the dc ($\delta = 0$) case the bulk electric fields vanish when the membrane is nonconducting, i.e., when $g_m = 0$. This is not the case for the oscillating components, as seen for example in their $\omega\to+\infty$ limit (full expressions are given in Appendix A):

$$\begin{aligned}E_{2,c,\omega\to+\infty}^{(0)} &= \frac{\sqrt{2}\delta}{1+S(1+\alpha)}, \quad E_{2,s,\omega\to+\infty}^{(0)} = 0,\\ E_{1,c,\omega\to+\infty}^{(0)} &= SE_{2,c,\omega\to+\infty}^{(0)}, \quad E_{1,s,\omega\to+\infty}^{(0)} = 0.\end{aligned} \tag{23}$$

The electric field in the base state generates a (rescaled) electric pressure on the (flat) membrane (12),

$$p^{{\rm el},(0)} = \tfrac{1}{2}\left[\left(E_{z,1}^{(0)}\right)^2 - S\left(E_{z,2}^{(0)2}\right)^2\right]. \tag{24}$$

This isotropic electric pressure is compensated by hydrostatic pressure, and the fluids are at rest in the base state. Moreover, since the electric stress has no tangential component, from the

tangential stress balance (4) it follows that the tension in the membrane is uniform at leading order: $\xi^{(0)} = \xi_0$.

B. Linearized evolution equations

In order to determine the perturbed electric potential, velocity, and pressure fields, we need to apply the boundary conditions at the deformed interface. All variables are expanded in Taylor series, and the boundary conditions are evaluated at $z = 0$:

$$u(z=h) = u(z=0) + h\frac{\partial u}{\partial z}\bigg|_{z=0} = u^{(0)}(z=0) + \left[u^{(1)}(z=0) + h\frac{\partial u^{(0)}}{\partial z}\bigg|_{z=0}\right]. \quad (25)$$

The solution for the perturbed potential yields [with boundary conditions $\phi^{(1)}(\pm\infty) = 0$]

$$\phi^{(1)}_{1q}(t) = A_{1q}(t)\exp(-qz), \quad \phi^{(1)}_{2q} = A_{2q}(t)\exp(qz). \quad (26)$$

We introduce A_{1q} and A_{2q} as the amplitudes of the potentials on each side of the membrane, which are unknown functions of time. The perturbed transmembrane potential is

$$V^{(1)}_{mq} = A_{2q} - A_{1q} + h_q\left(E^{(0)}_1 - E^{(0)}_2\right). \quad (27)$$

When dealing with simple interfaces, one typically uses h_q and the interfacial charge Q_q to characterize the state of the system [36,39]. Our problem is more complicated due to the potential discontinuity, and needs a third variable to be fully described. We choose to use h_q, A_{1q}, and A_{2q} (instead for example of h_q, V_{mq}, and Q_q) in order to obtain a more symmetric (and convenient to manipulate) set of equations. The current conservation (10) serves to relate A_{1q} and A_{2q} to h_q (through $V^{(1)}_{mq}$), and gives at first order

$$RA_{2q} + S\alpha\frac{dA_{2q}}{dt} = -A_{1q} - \alpha\frac{dA_{1q}}{dt}, \quad (28)$$

$$A_{1q} + \frac{dA_{1q}}{dt} = \frac{dV^{(1)}_{mq}}{dt} + g_m V^{(1)}_{mq}. \quad (29)$$

The kinematic condition (14) describes the evolution of the shape mode,

$$\frac{dh_q}{dt} = \beta f(q)[p^{\mathrm{el},(1)} - \mathrm{Ca}^{-1}(q^4 + \xi_0 q^2)h_q], \quad (30)$$

where

$$f(q) = \frac{\cosh 2q - 1 - 2q^2}{2(1+\lambda)q(2q + \sinh 2q)}. \quad (31)$$

In the absence of an electric field ($p^{\mathrm{el},(1)} = 0$), Eq. (30) describes the relaxation of shape perturbations towards a flat membrane, under the influence of elastic restoring forces. Considering a shape perturbation of the form $h_q(t) = \hat{h}_q e^{-st}$, two well-known limits may be recovered. The first one is the result of [48] for a tensionless ($\xi_0 = 0$ with our notations), symmetric ($\mu_1 = \mu_2$), and unbounded ($q \gg 1$) membrane, which in dimensional form is written as $s = -\kappa q^3/4\mu_1$, $q^{-1} \ll L$. In the opposite limit of a wall-bounded membrane, $q^{-1} \gg L$, we find $s = -\kappa L^3 q^6/12\mu_1$ in agreement with [49].

Equations (28), (29), and (30) describe the evolution of the linearly perturbed system. Details about the calculations are given in Appendixes B and C.

Equation (30) shows that the stability depends on the electric pressure in the perturbed state (12), which is

$$p^{\mathrm{el},(1)}_q = qE^{(0)}_1 A_{1q} + qSE^{(0)}_2 A_{2q}. \quad (32)$$

In (30), $f(q)$ is always positive: it scales as q^2 for small values of q, but decreases as $1/q$ when $q \gg 1$. The elastic term $-\mathrm{Ca}^{-1}(q^4 + \xi_0 q^2)h_q$ is always stabilizing (provided that the tension ξ_0 is positive): the q^4 contribution is due to bending, the q^2 term is due to tension, and both oppose deformation. On the contrary, electric pressure may become positive and destabilize the membrane. However, for $q \gg 1$ the elastic term dominates, so the membrane is always stable for sufficiently high wave numbers q.

The membrane experiences electric shear stresses as well:

$$\tau^{(1)}_{\mathrm{el},t} = E^{(0)}_{z,1}E^{(1)}_{x,1} + \frac{\partial h}{\partial x}\left(E^{(0)}_{z,1}\right)^2 - S\left[E^{(0)}_{z,2}E^{(1)}_{x,2} + \frac{\partial h}{\partial x}\left(E^{(0)}_{z,2}\right)^2\right] = -ip^{\mathrm{el},(1)}_q + 2iqh_q p^{\mathrm{el},(0)}, \quad (33)$$

but they are balanced by gradients in the membrane tension. The tension varies as $\xi = \xi_0 + \xi_q(t)e^{iqx}$, where the nonuniform part ξ_q is determined from the tangential stress balance $\tau_{\mathrm{el},t} = -\nabla_s\xi$, and

$$\xi_q = \frac{p^{\mathrm{el},(1)}_q}{q} - 2h_q p^{\mathrm{el},(0)}. \quad (34)$$

The perturbation in the tension does not enter the first-order normal stress balance and does not affect the shape evolution (30) (its contribution is second order).

C. Growth rate: Floquet analysis

When the electric fields $E^{(0)}_1$ and $E^{(0)}_2$ are constant in time (that is, when $\delta = 0$), the growth rate s of a given perturbation is found by looking for solutions of the form $h_q(t) = \hat{h}_q e^{st}$, $A_{iq}(t) = \hat{A}_{iq}e^{st}$, as in [25]. The growth rate s is then found analytically as the solution of a third-order polynomial equation.

This approach is not applicable when electric fields vary in time, which is the case of interest here. This is easily seen in Eq. (29), where $E^{(0)}_2(t)$ and $E^{(0)}_1(t)$ appear in the expression of $V^{(1)}_m$. However, since the forcing electric terms are periodic in time and our system is linear, we may use techniques derived from the Floquet theorem to compute the growth rate s of any perturbation. We will briefly outline these techniques here, mostly following Klausmeier [50] (see also [36,39,51]).

Let us first assume that our system can be written in a matrix form (the detailed transformation is given in Appendix D),

$$\frac{dX}{dt} = M(t)X, \quad (35)$$

where X is a vector of length n describing our system (in the present work $n = 3$ and the three elements of X are h_q, A_{1q}, and A_{2q}), and $M(t)$ is an $n \times n$ matrix which is T periodic in time (here $T = 2\pi/\omega$). The Floquet theorem states that the

general solution of Eq. (35) is

$$X(t) = \sum_{i=1}^{n} c_i e^{\zeta_i t} \mathbf{p}_i(t), \tag{36}$$

where the coefficients c_i depend on initial conditions. The vector-valued (here with three components) functions $\mathbf{p}_i$ are T periodic, which implies that their amplitude is finite and that the long-term stability of the system is entirely controlled by the real parts of the n Floquet exponents ζ_i: the growth rate of the system is $s_q = \max \mathrm{Re}(\zeta_i)$.

The challenge is to calculate these exponents numerically, and we employed two commonly used techniques. In the integration method, one first integrates Eq. (35) over one period, with the $n \times n$ identity matrix as initial condition, which is equivalent in practice to solving it n times with different initial vectors [(1,0,0), (0,1,0), and (0,0,1) in our case]. The Floquet multipliers $e^{\zeta_i t}$ are the eigenvalues of the resulting matrix $X(T)$.

The other method is often referred to as the Hill's method, and uses a Fourier decomposition of the T-periodic matrix M and the functions $\mathbf{p}_i$. Let us consider one Floquet exponent ζ. The corresponding $\mathbf{p}$ may be written as an infinite sum of its Fourier components: $\mathbf{p} = \sum_{k=-\infty}^{+\infty} \mathbf{p}_k e^{ik\omega t}$. In our system, this can be equivalently written in terms of our variables as (simply making explicit the three components of the vector-valued function $\mathbf{p}$, and of its Fourier components $\mathbf{p}_k$) $h_q = \sum_{k=-\infty}^{+\infty} h_k e^{ik\omega t} e^{\xi t}$, $A_{1q} = \sum_{k=-\infty}^{+\infty} a_{1k} e^{ik\omega t} e^{\zeta t}$, and $A_{2q} = \sum_{k=-\infty}^{+\infty} a_{2k} e^{ik\omega t} e^{\zeta t}$. These expressions are then introduced in Eq. (35) (where the T-periodic matrix M has also been expanded in Fourier series), and collecting coefficients in front of the same-order harmonics yields an eigenvalue problem of the form $M_\zeta X_\zeta = \zeta X_\zeta$. X_ζ is an infinite vector containing all the coefficients h_k, a_{1k}, and a_{2k} and accordingly M_ζ is an infinite matrix. Hence, there exist an infinite number of eigenvalues ζ. Given one solution, an infinite family of solutions can be generated by adding $i\omega$ to it an arbitrary number of times (which does not change its real part, but simply corresponds to a shift in phase of one period). And, in fact, the entire set of solutions forms n different families, each based on one of the "real" Floquet exponents of the system.

When solving the eigenvalue problem numerically, the Fourier decomposition is truncated at order N, and M_ζ (given for reference in Appendix D) becomes a finite matrix of size $(6N + 3) \times (6N + 3)$. Its $6N + 3$ eigenvalues are easily found using any computational tool and they can be separated into three families of $2N + 1$ solutions as shown in Fig. 2. The truncation errors show up in the fact that the solutions are not exactly separated by $i\omega$. Additionally, the eigenvalues' real parts are not exactly the same within each family: for the family with the largest real part in Fig. 2, they lie between 0.04 and 0.12. To improve the accuracy of this technique, we consider only approximately one-third of the total number of eigenvalues, those whose imaginary part is closest to zero, and average their real parts within each family. We thus get from the calculation three real numbers (corresponding to the computed real part of each Floquet exponent), and the largest one is chosen as the growth rate of the system.

In Hill's method the accuracy is very simply controlled by the truncation threshold N, whereas in the integration method it is controlled by the tolerance parameter of the integration scheme used (we used the ode45 solver of MATLAB software, based on an explicit Runge-Kutta formula). When comparing the two methods, we adjusted this tolerance parameter so that both of them achieved comparable computational speeds. In the dc case ($\delta = 0$), the results of the Floquet analysis with $N = 50$ agree with the analytical solution by Seiwert *et al.* [25] (the relative error is on the order of 10^{-12}). Although not shown, we checked that the calculations are converged for all values of the parameters (and in particular for $\delta > 0$). Throughout this study we preferentially used Hill's method, as we found its behavior to be more robust, and mostly used the integration method as a mean to check our results.

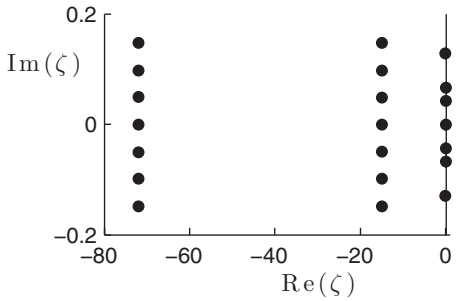

FIG. 2. Illustration of Hill's method (see text), for $q = 10$, $R = 10$, $S = 1$, $\omega = 1$, $\delta = 1$, $\mathrm{Ca} = 10^5$, $\beta = 1$, $g_m = 20$, $\alpha = 0.1$, $\lambda = 1$, and $\xi_0 = 0$. We plotted all the complex solutions ζ of the eigenvalue problem. For clarity, we kept only the first three modes of the Fourier series ($N = 3$), and accordingly there are $6 \times 3 + 3 = 21$ eigenvalues. The eigenvalues segregate into three distinct families of approximately equal real parts, and their imaginary parts should differ by $i\omega$ (here $\omega = 0.05$). This is not the case for the family with the highest real part: too few modes were taken into account to guarantee satisfactory precision of the calculations ($N = 50$ modes are used throughout this work).

IV. RESULTS

Typical values for the parameters in experiments with giant lipid vesicles are $R = 10$, $S = 1$, $\lambda = 1$, $\omega = 1$, $\mathrm{Ca} = 10^5$ (corresponding to electric field strengths of 1 kV/m), $\beta = 1$, $g_m = 0$, and $\alpha = 0.1$ [25,29]. To calculate some of this values, we considered $L \approx 100$ μm. Depending on the conductivity of the surrounding fluids, the capacitive charging time varies between 10^{-3} and 1 s. We will most often assume a purely sinusoidal potential, i.e., $\delta = 1$. The membrane tension in the absence of electric field can be as low as 10^{-9} N/m [52]; therefore, for simplicity, we consider an initially tension-free membrane, that is, $\xi_0 = 0$.

A. Effect of the ac field frequency

Before delving into the analysis of the effects of the time-varying electric field, we summarize a few important results in the dc case [25]. If displacement currents are negligible (equivalent to setting $\alpha = 0$), which is justified in most biological applications, the criterion for instability is $g_m(R - 1)(R^2 - S) > 0$. In the more general case $\alpha \neq 0$, there is no such simple criterion but instability always requires a conducting membrane ($g_m > 0$), and fluid properties (R and S)

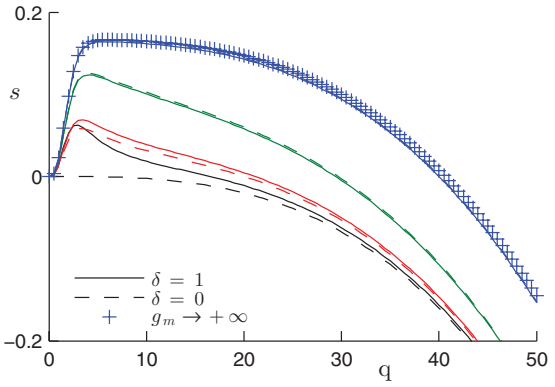

FIG. 3. (Color online) Growth rate s as a function of wave number q, for $R = 10, S = 1, \mathrm{Ca} = 10^5, \beta = 1, g_m = 0, \alpha = 0.1, \lambda = 1$, and $\xi_0 = 0$. Dashed lines correspond to dc electric field $\delta = 0$ and solid lines correspond to a sinusoidal electric field $\delta = 1$ with frequency $\omega = 3$. For each family of curves, g_m increases from bottom to top: $g_m = 0$ (black), 4 (red), 20, (green), and 1000 (blue). Note that, unlike what happens for a dc field, in the ac case an instability develops even for $g_m = 0$. As g_m increases, the ac and dc growth curves collapse (they become indistinguishable on the graph for $g_m > 20$): + symbols correspond to the $g_m \gg 1$ limit, which is the same for ac and dc fields.

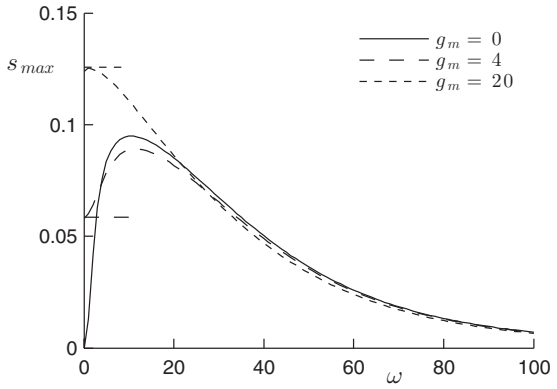

FIG. 4. Fastest growth rate $s_{\max}$ as a function of ω for $R = 10$, $S = 1, \delta = 1, \mathrm{Ca} = 10^5, \beta = 1, \alpha = 0.1, \lambda = 1, \xi_0 = 0$, and different values of g_m. The short horizontal lines starting at the origin of each curve represent the values calculated for the dc field $\delta = 0$.

within a certain range. In particular, there can be no instability if the fluids have equal conductivities, that is $R = 1$.

In contrast to the dc case, the membrane can be unstable in an ac field ($\delta = 1$) even for $g_m = 0$, due to the fact that the time-varying field generates currents in the system by alternatively charging and discharging the membrane over each period. Figure 3 compares the growth rate s as a function of wave number q for a dc and an ac electric field, and different values of g_m.

As g_m increases, both the extent of the unstable region and the maximum growth rate $s_{\max}$ increase, and the difference between the ac and dc results decreases. The latter effect reflects the fact that the current due to the charging of the membrane $\partial V_m/\partial t$ becomes negligible compared to the Ohmic current $g_m V_m$. As $g_m \to +\infty$ both growth curves converge towards the limit obtained for a dc field. This limit has a simple analytical expression when displacement currents are negligible ($\alpha s \ll 1$), which illustrates nicely the balance between the restoring elastic and the destabilizing electric forces:

$$s_{\alpha=0}^{g_m\to+\infty} = \beta f(q)\Big[q E_{2,\mathrm{dc}}^{(0)2}\frac{(R-1)(R^2-S)}{R+1} - \mathrm{Ca}^{-1}(q^4+\xi_0 q^2)\Big]. \tag{37}$$

As a conclusion, the effect of a varying electric field is most pronounced when the conductivity of the membrane is low, and for the rest of this study we will focus on $g_m = 0$.

The effect of the field frequency ω on the maximum growth rate $s_{\max}$ is illustrated in Fig. 4. It shows a nonmonotonic dependence, where at low frequencies $s_{\max}$ approaches its dc value and at high frequencies $s_{\max}$ vanishes independently of the membrane conductivity g_m.

Figures 3 and 4 also illustrate the typical values of the nondimensional instability characteristics: $s_{\max} \approx 0.1$, $q_{\max} \approx$ 1–10. For a giant lipid vesicle, these correspond to a most unstable wavelength of 1–100 μm.

1. *Instability at high frequencies $\omega \gg 1/\alpha$*

Figure 4 shows that at high frequencies, the maximum growth rate $s_{\max}$ decreases but remains positive, implying instability. In this frequency regime the period of the field oscillations becomes shorter than the bulk charging time, i.e., $\omega \gg 1/\alpha$, and the system is dominated by displacement currents. The base electric fields reduce to (in the case of $\delta = 1$)

$$E_2^{(0)} = \frac{\sqrt{2}}{1+S+\alpha S}\cos\omega t, \quad E_1^{(0)} = S E_{2,c}^{(0)}. \tag{38}$$

The fact that the electric fields do not depend on R or g_m anymore is a consequence of the prevalence of displacement currents. By assuming that each variable varies on the same time scale as the electric field, so that it is negligible compared to its derivative when $\omega \gg 1/\alpha$, the continuity of bulk currents across the membrane becomes

$$\alpha\frac{dA_{1q}}{dt} = -\alpha S\frac{dA_{2q}}{dt}, \quad \text{i.e.,} \quad A_{1q} = -SA_{2q}, \tag{39}$$

whereas the continuity of bulk and membrane currents gives

$$\begin{aligned} -(\alpha q S + 1 + S)\frac{dA_{2q}}{dt} &= \frac{dh_q}{dt}\left(E_1^{(0)} - E_2^{(0)}\right) \\ &= \frac{dh_q}{dt}E_2^{(0)}(S-1), \\ A_{2q} &= -\frac{h_q E_2^{(0)}(S-1)}{\alpha q S + 1 + S} + K_1. \end{aligned} \tag{40}$$

The constant K_1 can be found from the initial values of A_{2q} and h_q, and it is neglected since we focus on unstable modes (for which h_q diverges). The evolution equation for h_q is thus

$$\frac{dh_q}{dt} = \beta f h_q\left(qS\frac{\left(E_2^{(0)}\right)^2(S-1)^2}{\alpha q S + 1 + S} - \mathrm{Ca}^{-1}(q^4+\xi_0 q^2)\right). \tag{41}$$

This equation has a simple analytical solution, since $E_2^{(0)}$ is a sinusoidal function, and the growth rate s can be instantly

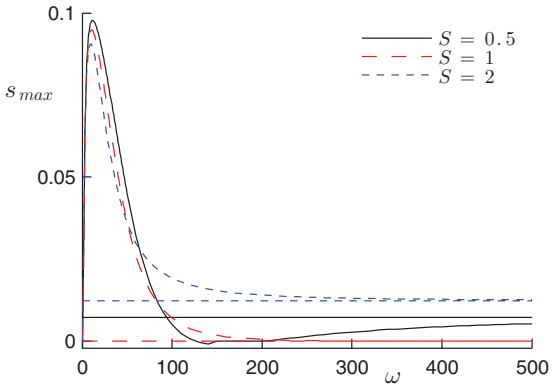

FIG. 5. (Color online) Maximum growth rate $s_{\max}$ as a function of ω for $R = 10$, $\delta = 1$, $\mathrm{Ca} = 10^5$, $\beta = 1$, $g_m = 0$, $\alpha = 0.1$, $\lambda = 1$, $\xi = 0$, and different values of S. The horizontal lines are calculated from the approximate solution (42).

recovered by averaging the equation over one period

$$s = \beta f\left(qS\frac{(S-1)^2}{\alpha q S + 1 + S}\langle E_2^{(0),2}\rangle - \mathrm{Ca}^{-1}(q^4 + \xi_0 q^2)\right), \quad (42)$$

where $\langle\cdots\rangle$ denotes time averaging over a period. The electric field contribution in Eq. (42) (the first term on the right-hand side) is always positive, and thus destabilizing. It is also dominant at small q; thus it follows that the membrane is always unstable in the high-frequency regime as long as $S \neq 1$ (as seen in Fig. 5).

2. *Intermediate values of ω*

An important conclusion is drawn from the results in the previous section: the membrane can always be made unstable by increasing the frequency of the field, provided that the liquids have different permittivities ($S \neq 1$). For $S = 1$ and $g_m > 0$, the membrane is unstable for very low frequencies (in the dc limit), provided that the liquids have different conductivities ($R \neq 1$). However, the membrane is always stable in the case of symmetric fluids, $R = S = 1$.

In most biologically relevant situations $S \approx 1$ and thus the membrane is stable at high frequencies. Moreover, at low frequencies the membrane is also expected to be stable because an intact lipid membrane has negligible conductivity ($g_m \ll 1$). The question arises of whether the membrane is still stable at intermediate frequencies. To answer this question, we present an approximate analytical solution of our system, valid for $\omega \ll 1/\alpha$. Displacement currents may then be neglected, which corresponds to setting $\alpha = 0$ in the evolution equations. This greatly simplifies the relation between the electric fields in the fluids on either side of the membrane, giving for the base and linearly perturbed states

$$E_1^{(0)} = RE_2^{(0)}, \quad A_{1q} = -RA_{2q}. \quad (43)$$

The simplicity of these relations makes it convenient to use the transmembrane potential as a variable: $V_{mq}^{(1)} = A_{2q}(R+1) + h_q E_2^{(0)}(R-1)$. The system (28), (29), and (30) thus reduces

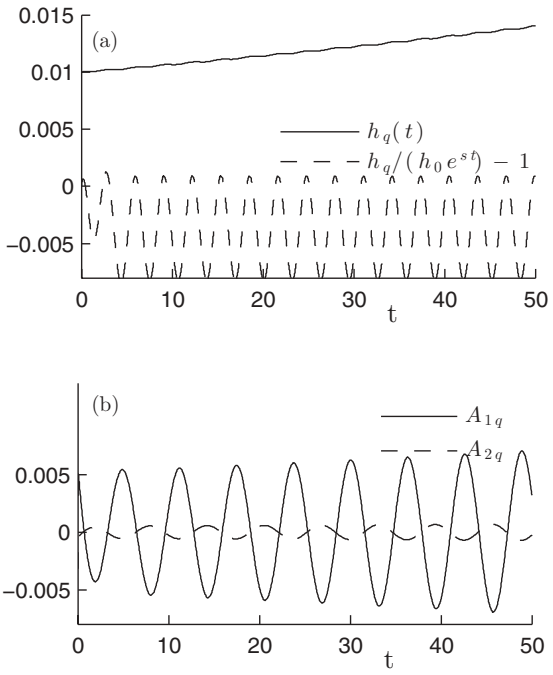

FIG. 6. Numerical integration of the system of equations (28), (29), and (30), for $R = 10$, $S = 1$, $\omega = 1$, $\delta = 1$, $\mathrm{Ca} = 10^5$, $\beta = 1$, $g_m = 0$, $\alpha = 0.1$, $\lambda = 1$, and $\xi = 0$. (a) Evolution of h_q (solid lines). Dashed lines represent the normalized variation around an exponential growth, which is within 1% of h_q. (b) In contrast, A_{1q} and A_{2q} vary almost sinusoidally around 0 (with a slowly growing amplitude).

to two coupled equations:

$$\frac{dh_q}{dt} = \beta f\left(q\left(E_2^{(0)}\right)^2\frac{(R-1)(R^2-S)}{R+1} - \mathrm{Ca}^{-1}(q^4+\xi q^2)\right)h_q - \beta f q E_2^{(0)}\frac{R^2-S}{R+1}V_{mq}^{(1)}, \quad (44)$$

$$\frac{dV_{mq}^{(1)}}{dt} = -\frac{qR + g_m(1+R)}{1+R}V_{mq}^{(1)} + qRE_2^{(0)}\frac{R-1}{R+1}h_q. \quad (45)$$

We further assume that h_q varies exponentially: $h_q = \hat{h}e^{s_q t}$. Although it is difficult to provide a proof of validity for this approximation, it holds empirically very well throughout the range of parameters used in this work. As seen in Fig. 6, the amplitude of the oscillating part of h_q is typically 1% of its value. In contrast, A_{1q} and A_{2q}, for example, vary almost sinusoidally around 0 with a slowly growing amplitude [Fig. 6(b)].

This assumption allows us to calculate (easily, albeit tediously) $V_{mq}^{(1)}$ from Eq. (45), and insert it in (44). The right-hand side of (44) oscillates with a frequency ω (due to the terms containing $V_{mq}^{(1)}$ or $E_2^{(0)}$). We lastly assume $s \ll \omega$, and average the equation over one period. This leads to a fourth-order polynomial equation for s,

$$s = \beta f q^2 R\frac{(R-1)(-R^2+S)}{(R+1)^2} \times \frac{(s+K)^2\langle E_2^{(0)2}\rangle + \omega^2 E_{\mathrm{dc}}^{(0)2}}{(s+K)^3 + \omega^2(s+K)} + s_0, \quad (46)$$

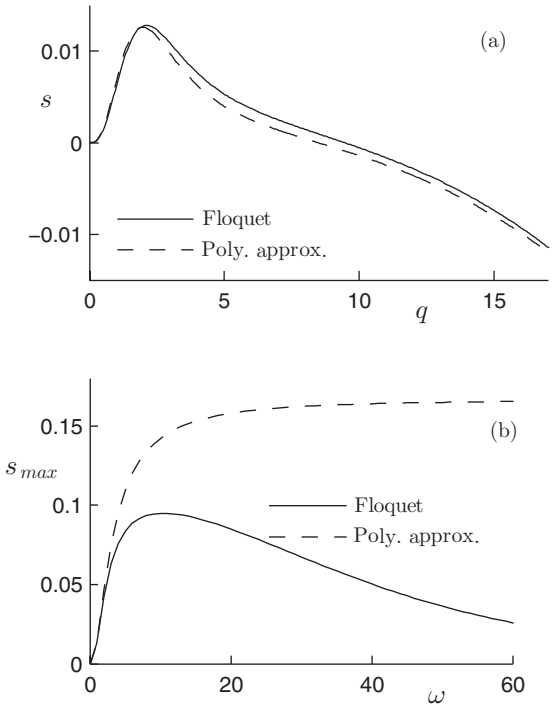

FIG. 7. (a) Growth rate as a function of wave number for $R = 10$, $S = 1$, $\omega = 1$, $\delta = 1$, $\mathrm{Ca} = 10^5$, $\beta = 1$, $g_m = 0$, $\alpha = 0.1$, $\lambda = 1$, and $\xi_0 = 0$. (b) shows the largest growth rate as a function of ω. In both figures, the solid line is the result of the Floquet analysis, while the dashed line represents the approximate solution (46). As expected, the latter is valid only for low frequencies ($\omega < 1/\alpha$), since it does not take into account displacement currents.

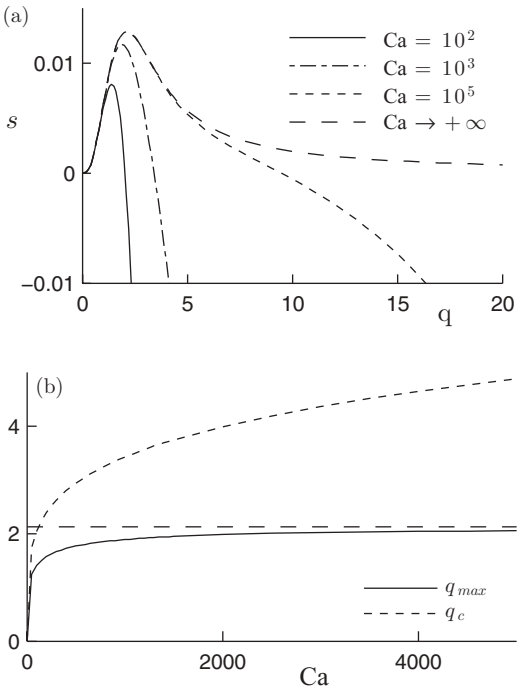

FIG. 8. Properties of the instability for $R = 10$, $S = 1$, $\omega = 1$, $\delta = 1$, $\beta = 1$, $g_m = 0$, $\alpha = 0.1$, $\lambda = 1$, and $\xi = 0$. (a) Growth rate s as a function of q, for increasing values of Ca. The growth rate converges towards a limit curve (dashed line), which is calculated numerically by setting $\mathrm{Ca}^{-1} = 0$ in the system of equations. (b) Whereas the most unstable wave number $q_{\max}$ (and $s_{\max}$) converges towards a finite value, the highest unstable wave number q_c diverges as $\mathrm{Ca} \to +\infty$.

where

$$K = \frac{qR + g_m(1+R)}{1+R} \tag{47}$$

and

$$s_0 = \beta f q \frac{(R-1)(R^2-S)}{R+1}\langle E_2^{(0)2}\rangle - \beta f \mathrm{Ca}^{-1}(q^4 + \xi q^2). \tag{48}$$

Figure 7 compares the growth rate obtained from this polynomial approximation with the Floquet analysis for a system with $\alpha = 0.1$. As expected, both agree for $\omega \leqslant 10$, or $\alpha\omega \leqslant 1$. For higher values of ω, the approximate solution has a totally different behavior; $s_{\max}$ reaches a plateau $s_{\max} \approx 0.15$, whereas the true solution vanishes. This discrepancy is obviously due to the neglected displacement currents in the approximate solution.

For our discussion, let us consider the long-wavelength limit of our approximation $q \ll 1$, where the growth rate is simply

$$s = \beta f q \frac{(R-1)(R^2-S)}{R+1}\langle E_2^{(0)2}\rangle. \tag{49}$$

Although this result is an approximation, it is very robust since ω and q can be chosen independently as to satisfy the assumptions $s \ll \omega \ll 1/\alpha$. It proves that the membrane is unstable when $(R-1)(R^2-S) > 0$ and $\langle (E_2^{(0)})^2\rangle \neq 0$. This is always the case when $S = 1$ and $R \neq 1$, as long as $\delta \neq 0$. Going back to the discussion at the beginning of this section, it means that by a careful choice of the frequency of the field, a biomembrane can always be made unstable, unless $R = S = 1$ (in which case the two surrounding fluids are electrically the same).

B. Effect of electric field strength: Ca and β

Experimentally, the easiest way to enhance the instability is to increase the applied voltage. With our rescaling, this means increasing β and Ca, which both scale as V_0^2, but to simplify the discussion, we will consider each of them separately. Figure 8 illustrates the effect of Ca. The growth rate s increases with this parameter and tends towards a limit curve [dashed line in Fig. 8(a)], which is calculated numerically by setting $\mathrm{Ca}^{-1} = 0$ in Eq. (30). Physically, this limit corresponds to neglecting all mechanical restoring forces of the membrane (tension and bending resistance): the problem simplifies to a balance between electric and viscous stresses. Since there are no restoring processes, the stability is entirely determined by the sign of the electric pressure, which is destabilizing for the set of parameters shown; the growth rate is always positive. An important consequence, as seen in Fig. 8(b), is that the extent of the unstable wavelengths diverges with Ca (that is, the largest unstable mode q_c tends to $+\infty$). In contrast, both the largest growth rate $s_{\max}$ and the most unstable wave number $q_{\max}$ approach a finite value. Indeed, once the elasticity of the membrane becomes negligible, the interface dynamics is controlled by the electric pressure and must be independent of

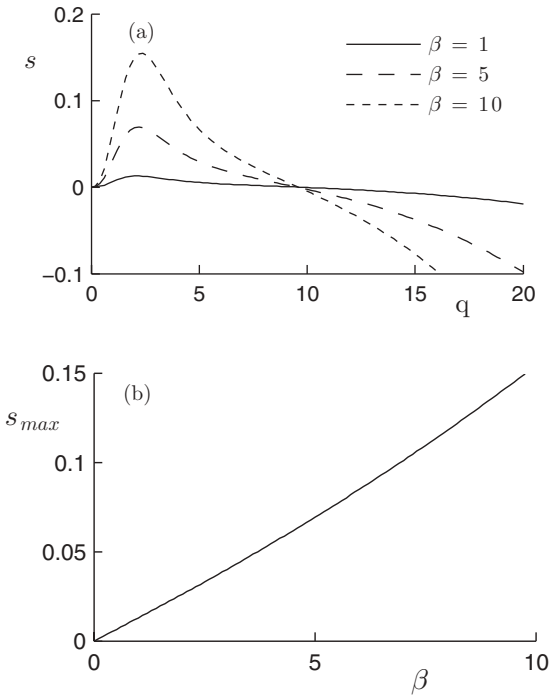

FIG. 9. Properties of the instability for $R = 10$, $S = 1$, $\omega = 1$, $\delta = 1$, $\mathrm{Ca} = 10^5$, $g_m = 0$, $\alpha = 0.1$, $\lambda = 1$, and $\xi = 0$. (a) Growth rate s as a function of q, for increasing values of β. The fastest growing wave number and the extent of the unstable region are almost independent of β. (b) The maximum growth rate $s_{\max}$, however, increases almost linearly with β.

Ca. Typical biophysics experiments, with $\mathrm{Ca} \approx 10^5$, lie just at the edge of this plateau regime.

Figure 9 shows that increasing β affects the most unstable and the highest unstable wave numbers very little. Figure 9(b) shows that the maximum growth rate, however, increases almost linearly with β. This behavior is illustrated by (30), where β appears as a multiplication factor of dh_q/dt.

V. CONCLUSIONS

We have analyzed the destabilization of a bilayer membrane by the electric pressure generated by a uniform ac electric field. The main result is that while an insulating membrane is linearly stable in dc electric fields, using ac fields, the membrane can always be made unstable, except for the symmetric case of a membrane separating the same fluids $R = S = 1$. In the present model, at very low frequencies the instability is controlled by the dc field criterion $g_m(R-1)(R^2-S) > 0$ [25]. At intermediate frequencies ($\omega \ll 1/\alpha$), the instability appears when $(R-1)(R^2-S) > 0$. And at large frequencies ($\omega \gg 1/\alpha$), the membrane is unstable with a growth rate proportional to $(S-1)^2$.

This discussion takes into account only the destabilization due to the electric pressure produced by the electric field. It would be very interesting to see how other mechanisms of instability, such as electric-field-induced negative tension (as studied in [18] for a dc field) and electrokinetic flows [19], are affected by an ac field.

ACKNOWLEDGMENTS

This work was partially supported by NSF Awards No. CBET-1117099 and No. CBET-1132614.

APPENDIX A: ELECTRIC FIELDS IN THE BASE STATE

To calculate the electric fields in the base state, we consider independently the dc and ac parts of the potential $V = \sqrt{1-\delta^2} + \delta\sqrt{2}\,\cos\omega t$ to find the corresponding parts of the electric fields.

1. dc potential

Let us first consider an applied dc potential $V(t) = 1$. To find the dc part of the fields, we will just multiply the result by $\sqrt{1-\delta^2}$. In each fluid, $k = 2,1$, the potential ϕ_k is solution of the Laplace equation $\nabla^2\phi_k = 0$. The potential is imposed at the electrodes $[\phi(z = \pm 1,t) = \mp 1/2]$, which gives

$$\phi_1(z) = -1/2 + \beta_1(z-1), \quad \phi_2(z) = 1/2 + \beta_2(z+1). \tag{A1}$$

In the case of fast bulk charge relaxation, $\alpha = 0$, the conservation of bulk currents reduces to $RE_2(0) = E_1(0)$, or

$$R\beta_2 = \beta_1. \tag{A2}$$

The transmembrane potential is $V_m = \phi_2(0,t) - \phi_1(0,t) = 1 + \beta_2(1+R)$. The equation for V_m from the continuity of bulk and membrane currents becomes

$$\frac{dV_m}{dt} + \frac{R + g_m(1+R)}{1+R} V_m = \frac{R}{1+R}, \tag{A3}$$

which yields

$$V_m(t) = \frac{R}{R + g_m(1+R)}(1 - e^{-t/t_m}), \tag{A4}$$

where the (nondimensional) charging time for a leaky capacitive membrane is

$$t_m = \frac{(1+R)}{R + g_m(1+R)}. \tag{A5}$$

At steady state, $V_m = R/[R + g_m(1+R)]$, which gives the dc part of the electric fields,

$$E_{1,\mathrm{dc}} = \frac{Rg_m\sqrt{1-\delta^2}}{R + g_m(1+R)}, \quad E_{2,\mathrm{dc}} = \frac{g_m\sqrt{1-\delta^2}}{R + g_m(1+R)}. \tag{A6}$$

2. ac potential

Let us now consider a sinusoidal potential $V = \cos\omega t$. We use complex notation to find the electric field and write the potential as $\phi = \underline{\Phi} e^{i\omega t}$. The Laplace equation becomes $\Delta\underline{\Phi} = 0$; together with the continuity of potential at the electrodes it imposes:

$$\underline{\Phi}_1(z,t) = -1/2 + \underline{B}_1(z-1), \quad \underline{\Phi}_2(z,t) = 1/2 + \underline{B}_2(z+1). \tag{A7}$$

Conservation of bulk currents imposes

$$RE_2 + \alpha S \partial_t E_2 = E_1 + \alpha \partial_t E_1,$$
$$(R + i\alpha S\omega)\underline{B}_2 = (1 + i\alpha\omega)\underline{B}_1,$$
$$\underline{B}_1 = \underline{R}B_2 \quad \text{with} \quad \underline{R} = \frac{R + i\alpha\omega S}{1 + i\alpha\omega}. \tag{A8}$$

The continuity of bulk and membrane currents becomes $-(R + i\alpha\omega S)B_2 = d_t V_m + g_m V_m$, with $\underline{V}_m = 1 + \underline{B}_2(1 + \underline{R})$. Simple substitution gives

$$\underline{B}_2 = -\frac{g_m + i\omega}{R + i\alpha\omega S + (g_m + i\omega)(1 + \underline{R})}. \tag{A9}$$

We write the electric fields as $E_k = E_{k,c}\cos\omega t + E_{k,s}\sin\omega t$ with the amplitudes of the sine and the cosine components given below for reference:

$$E^{(0)}_{2,c} = \sqrt{2}\delta \frac{g_m[R + g_m(1 + R)] + \alpha^2\omega^4[1 + S + \alpha S] + \omega^2[1 + R + \alpha S] + \alpha^2\omega^2 g_m[R + g_m(1 + S)]}{[R + g_m(1 + R) - \alpha^2\omega^2 S - \omega^2\alpha(S + 1)]^2 + \omega^2[1 + R + \alpha(R + S) + \alpha g_m(S + 1)]^2},$$
$$E^{(0)}_{2,s} = \sqrt{2}\delta\omega \frac{\alpha S\left[\omega^2(1 + \alpha^2 g_m) + g_m + g_m^2\right] - R\left[1 + \alpha g_m^2 + \alpha\omega^2(1 + \alpha)\right]}{[R + g_m(1 + R) - \alpha^2\omega^2 S - \omega^2\alpha(S + 1)]^2 + \omega^2[1 + R + \alpha(R + S) + \alpha g_m(S + 1)]^2}, \tag{A10}$$
$$E^{(0)}_{1,c} = \frac{(R + S\alpha^2\omega^2)E^{(0)}_{2,c} - \alpha\omega(R - S)E^{(0)}_{2,s}}{1 + \alpha^2\omega^2}, \quad E^{(0)}_{1,s} = \frac{(R + S\alpha^2\omega^2)E^{(0)}_{2,s} + \alpha\omega(R - S)E^{(0)}_{2,c}}{1 + \alpha^2\omega^2}.$$

APPENDIX B: FLOW AROUND THE MEMBRANE AT FIRST ORDER

The velocity field in a bounded domain is

$$v_{q,z,2} = iq\{-C_q q(z + 1)\cosh[q(z + 1)] + [C_q + D_q(1 + z)]\sinh[q(z + 1)]\},$$
$$v_{q,x,2} = \{D_q q(z + 1)\cosh[q(z + 1)] + [D_q - C_q q^2(1 + z)]\sinh[q(z + 1)]\}, \tag{B1}$$

$$v_{q,z,1} = iq\{-M_q q(z - 1)\cosh[q(z - 1)] + [M_q + N_q(z - 1)]\sinh[q(z - 1)]\},$$
$$v_{q,x,1} = \{N_q q(z - 1)\cosh[q(z - 1)] + [N_q - M_q q^2(z - 1)]\sinh[q(z - 1)]\}. \tag{B2}$$

It satisfies the no-slip boundary condition at the electrodes $z = \pm 1$. The corresponding pressure field is

$$p_{q,1} = 2iq\{M_q q\cosh[q(z - 1)] + N_q\sinh[q(z - 1)]\},$$
$$p_{q,2} = 2iq\{C_q q\cosh[q(z + 1)] + D_q\sinh[q(z + 1)]\}. \tag{B3}$$

In the Monge representation, $z = h(x,t)$, and with Fourier mode decomposition, the kinematic condition (14) becomes

$$\frac{dh_q}{dt} = v_{q,z} - iq v_{q,x} h_q. \tag{B4}$$

Since the leading-order velocity field is zero (hydrostatic equilibrium around a flat membrane), we have simply

$$\frac{dh_q}{dt} = v^{(1)}_{z,q} = M_q \frac{iq[\cosh(2q) - 2q^2 - 1]}{2(q\cosh q + \sinh q)}. \tag{B5}$$

The continuity of normal velocity yields $C_q = -M_q$. The area incompressibility requires that $v^{(1)}_x = 0$. Hence,

$$D_q = N_q = -M_q \frac{q^2}{q\coth q + 1}. \tag{B6}$$

M_q is determined from the normal stress balance

$$\left(T^{\mathrm{hd},(1)}_{zz,1} - T^{\mathrm{hd},(1)}_{zz,2}\right) + \left(p^{\mathrm{el},(1)}_q - \tau^{\mathrm{mm}}_{z,q}\right) = 0, \tag{B7}$$

where $\tau^{\mathrm{mm}} = \tau_\kappa + \tau_\Sigma$. Then

$$M_q = -i(1 + \lambda)^{-1}\frac{q\cosh q + \sinh q}{q^2[2q + \sinh(2q)]} \times \left[p^{\mathrm{el},(1)}_q + \frac{\kappa}{\epsilon_1 E_0^2 L^3}(q^4 + \xi_0 q^2)h_q\right]. \tag{B8}$$

The tangential stress balance

$$\left(T^{\mathrm{hd},(1)}_{xz,1} - T^{\mathrm{hd},(1)}_{xz,2}\right) + \left(\tau^{\mathrm{el},(1)}_{t,q} - \tau^{\mathrm{mm}}_{x,q}\right) = 0 \tag{B9}$$

serves to determine the nonuniform membrane tension which influences the dynamics at next order. From $\tau^{\mathrm{mm}}_{x,q} = iq\Sigma_q$ we find $\Sigma_q(t) = (R^2 - S)E^{(0)}_1(t)[A_q(t) + E^{(0)}_1(t)h_q(t)]$.

APPENDIX C: MEMBRANE STRESSES

The general formula for the bending tractions is given by (5). Since our problem is invariant in the y direction, the Gaussian curvature vanishes. On the other hand, the mean curvature H is a first-order quantity: $H = \frac{1}{2}\nabla\cdot\mathbf{n} \approx -\frac{q^2}{2}h_q$. Hence, when evaluated at first order, the bending stresses are

$$\boldsymbol{\tau}^{(1)}_\kappa = -\mathrm{Ca}^{-1}q^4 h_q\hat{\mathbf{z}}. \tag{C1}$$

The tension stresses in dimensionless form are

$$\boldsymbol{\tau}_\Sigma = \mathrm{Ca}^{-1}(2\xi H\mathbf{n} - \nabla_s\xi). \tag{C2}$$

At first order, the normal part of this stress only depends only on the value of the tension in the base state, which is constant, ξ_0. Thus,

$$\boldsymbol{\tau}^{(1)}_\Sigma = -\mathrm{Ca}^{-1}(\xi_0 q^2\hat{\mathbf{z}} + iq\xi_q\hat{\mathbf{x}})h_q. \tag{C3}$$

APPENDIX D: FLOQUET ANALYSIS

1. Dynamical system

In Sec. III B we wrote the evolution equations determining the stability of the system as

$$\frac{dh_q}{dt} = \beta f(q)\big[qE_1^{(0)}A_{1q} + qSE_2^{(0)}A_{2q} - \mathrm{Ca}^{-1}(q^4+\xi_0 q^2)h_q\big], \tag{D1}$$

$$A_{1q} + \alpha\frac{A_{1q}}{dt} = -RA_{2q} - \alpha S\frac{A_{2q}}{dt}, \tag{D2}$$

$$V_{mq}^{(1)} = A_{2q} - A_{1q} + h_q\big(E_1^{(0)} - E_2^{(0)}\big), \tag{D3}$$

$$A_{1q} + \frac{dA_{1q}}{dt} = \frac{dV_{mq}^{(1)}}{dt} + g_m V_{mq}^{(1)}. \tag{D4}$$

However, Fourier analysis requires a linear first-order equation system. We thus rewrite our system (with $\Delta E = E_1^{(0)} - E_2^{(0)}$) as

$$d_t h_q = \beta f(q)\big[qE_1^{(0)}A_{1q} + qSE_2^{(0)}A_{2q} - \mathrm{Ca}^{-1}(q^4+\xi_0 q^2)h_q\big], \tag{D5}$$

$$\begin{aligned}&\alpha(\alpha qS+1+S)\partial_t A_{2q}\\ &\quad= -\alpha h_q(\partial_t\Delta E + g_m\Delta E - fb\Delta E)\\ &\quad -A_{2q}\big(\alpha qR + R + \alpha g_m + \alpha Sfq E_2^{(0)}\Delta E\big)\\ &\quad -A_{1q}\big(1-\alpha g_m + \alpha fq E_1^{(0)}\Delta E\big),\end{aligned} \tag{D6}$$

$$\begin{aligned}&\alpha(\alpha qS+1+S)\partial_t A_{1q}\\ &\quad= \alpha S h_q(\partial_t\Delta E + g_m\Delta E - fb\Delta E)\\ &\quad +A_{2q}\big(-R + g_m\alpha S + \alpha S^2 fq E_2^{(0)}\Delta E\big)\\ &\quad -A_{1q}\big(\alpha qS + 1 + g_m\alpha S - \alpha Sfq E_1^{(0)}\Delta E\big),\end{aligned} \tag{D7}$$

where $b = \mathrm{Ca}^{-1}(q^4+\xi_0 q^2)$. This system can be written in matrix form $\frac{dX}{dt} = M(t)X$, where X is a three-component vector (h_q, A_{1q}, A_{2q}).

2. Hill's analysis

The Floquet theorem tells us that for each fundamental solution of the system, h_q, A_{1q}, and A_{2q} can be written as $\mathrm{Re}[h_{q,T}(t)e^{\zeta t}]$, $\mathrm{Re}[A_{1q,T}(t)e^{\zeta t}]$, and $\mathrm{Re}[A_{2q,T}(t)e^{\zeta t}]$, where the subscript T denotes a periodic function. The Floquet exponents ζ (which are complex) control the stability of the solution, and there is one per fundamental solution, that is, three in our system. The first method that we used to find those requires integration of the system numerically over one period, and is described in the text.

The second method uses a Fourier decomposition of the periodic functions (called Hill's decomposition):

$$h_{q,T} = \sum_{-\infty}^{\infty} h_k e^{ik\omega t}, \quad A_{1q,T} = \sum_{-\infty}^{\infty} a_{1,k}e^{ik\omega t}, \quad A_{2q,T} = \sum_{-\infty}^{\infty} a_{2,k}e^{ik\omega t}. \tag{D8}$$

These expressions are then substituted into the set of equations (D5)–(D7). Coupling between different modes of the Fourier decomposition appears whenever a variable (h_q, A_{1q}, or A_{2q}) is multiplied by an (oscillating) electric term. As an example, we list below the product of a generic variable g_q and a simple sinusoidal electric field with frequency ω, in terms of Fourier components. Notice that sub- and superharmonic terms are generated:

$$\begin{aligned}&g_{q,T}(E_c\cos\omega t + E_s\sin\omega t)\\ &= \sum_{-\infty}^{\infty}\left(g_k E_c\frac{e^{i(k+1)\omega t}+e^{i(k-1)\omega t}}{2} + g_k E_s\frac{e^{i(k+1)\omega t}-e^{i(k-1)\omega t}}{2i}\right)\\ &= \sum_{-\infty}^{\infty} e^{ik\omega t}\left(g_{k-1}\frac{E_c - iE_s}{2} + g_{k+1}\frac{E_c+iE_s}{2}\right).\end{aligned} \tag{D9}$$

Collecting terms in the same power of $e^{i\omega t}$ yields an eigenvalue equation of the form $\zeta X_\zeta = M_\zeta X_\zeta$ where X_ζ contains all the Fourier coefficients of h_q, A_{1q}, and A_{2q} and is of infinite size. To solve this equation and find the values of ζ (the method is specified in the text), the Fourier decomposition is truncated at order N. X_ζ is then of length $6N+3$, and is written $X_\zeta = (h_{-N}, h_{-N+1}, \ldots, h_{N-1}, h_N, a_{1,-N}, \ldots, a_{1,N}, a_{2,-N}, \ldots, a_{2,N})$. To write the coefficients of the matrix M_ζ, it is convenient to introduce simplified notations for the electric fields and their products:

$$\begin{aligned}&E_i^{(0)} = E_{i,\mathrm{dc}}^{(0)} + E_{i,c}^{(0)}\cos\omega t + E_{i,s}^{(0)}\sin\omega t, \quad \Delta E = E_1^{(0)} - E_2^{(0)} = \hat{E}_{\mathrm{dc}} + \hat{E}_c\cos\omega t + \hat{E}_s\sin\omega t,\\ &E_i^{(0)}\Delta E = \tilde{E}_{i,\mathrm{dc}} + \tilde{E}_{i,c}\cos\omega t + \tilde{E}_{i,s}\sin\omega t + \tilde{E}_{i,2c}\cos 2\omega t + \tilde{E}_{i,2s}\sin 2\omega t.\end{aligned} \tag{D10}$$

As an illustration, we list the dc parts of ΔE and $E_i^{(0)}\Delta E$:

$$\hat{E}_{\mathrm{dc}} = E_{1,\mathrm{dc}}^{(0)} - E_{2,\mathrm{dc}}^{(0)}, \quad \tilde{E}_{i,\mathrm{dc}} = E_{i,\mathrm{dc}}^{(0)}\hat{E}_{\mathrm{dc}} + \frac{E_{i,c}^{(0)}\hat{E}_c + E_{i,s}^{(0)}\hat{E}_s}{2}. \tag{D11}$$

The coefficients of M_ζ can then easily be deduced from the following relations, valid for $-N \leqslant k \leqslant N$ [for compactness, $b = \mathrm{Ca}^{-1}(q^4+\xi_0 q^2)$]:

$$\begin{aligned}\zeta h_k &= -h_k(\beta f b + ik\omega) + \beta fqa_{1,k}E_{1,\mathrm{dc}} + \beta fqa_{1,k-1}\frac{E_{1,c}-iE_{1,s}}{2} + \beta fqa_{1,k+1}\frac{E_{1,c}+iE_{1,s}}{2}\\ &+ \beta fqSa_{2,k}E_{2,\mathrm{dc}} + \beta fqSa_{2,k-1}\frac{E_{2,c}-iE_{2,s}}{2} + \beta fqSa_{2,k+1}\frac{E_{2,c}+iE_{2,s}}{2},\end{aligned} \tag{D12}$$

$$\begin{aligned}\zeta a_{2,k} = &-h_k\frac{(g_m-\beta f b)\hat{E}_{\rm dc}}{(\alpha q S+1+S)} - h_{k+1}\frac{\omega\hat{E}_s+(g_m-\beta f b)\hat{E}_c-i\omega\hat{E}_c+i(g_m-\beta f b)\hat{E}_s}{2(\alpha q S+1+S)}\\
&- h_{k-1}\frac{\omega\hat{E}_s+(g_m-\beta f b)\hat{E}_c+i\omega\hat{E}_c-i(g_m-\beta f b)\hat{E}_s}{2(\alpha q S+1+S)} - a_{2,k}\left(\frac{\alpha q R+R+\alpha g_m+\alpha S\beta f q\tilde{E}_{2,\rm dc}}{\alpha(\alpha q S+1+S)}+ik\omega\right)\\
&- \alpha S\beta f q a_{2,k+1}\frac{\tilde{E}_{2,c}+i\tilde{E}_{2,s}}{2\alpha(\alpha q S+1+S)} - \alpha S\beta f q a_{2,k-1}\frac{\tilde{E}_{2,c}-i\tilde{E}_{2,s}}{2\alpha(\alpha q S+1+S)} - \alpha S\beta f q a_{2,k+2}\frac{\tilde{E}_{2,2c}+i\tilde{E}_{2,2s}}{2\alpha(\alpha q S+1+S)}\\
&- \alpha S\beta f q a_{2,k-2}\frac{\tilde{E}_{2,2c}-i\tilde{E}_{2,2s}}{2\alpha(\alpha q S+1+S)} - a_{1,k}\frac{1-\alpha g_m+\alpha\beta f q\tilde{E}_{1,\rm dc}}{\alpha(\alpha q S+1+S)} - \alpha\beta f q a_{1,k+1}\frac{\tilde{E}_{1,c}+i\tilde{E}_{1,s}}{2\alpha(\alpha q S+1+S)}\\
&- \alpha\beta f q a_{1,k-1}\frac{\tilde{E}_{1,c}-i\tilde{E}_{1,s}}{2\alpha(\alpha q S+1+S)} - \alpha\beta f q a_{1,k+2}\frac{\tilde{E}_{1,2c}+i\tilde{E}_{1,2s}}{2\alpha(\alpha q S+1+S)} - \alpha\beta f q a_{1,k-2}\frac{\tilde{E}_{1,2c}-i\tilde{E}_{1,2s}}{2\alpha(\alpha q S+1+S)},\end{aligned} \tag{D13}$$

$$\begin{aligned}\zeta a_{1,k} = &\,h_k\frac{(g_m-\beta f b)d_{E\rm dc}}{\alpha q S+1+S}h_{k+1}\frac{\omega\hat{E}_s+(g_m-\beta f b)\hat{E}_c-i\omega\hat{E}_c+i(g_m-\beta f b)\hat{E}_s}{2(\alpha q S+1+S)}\\
&+ h_{k-1}\frac{\omega\hat{E}_s+(g_m-\beta f b)\hat{E}_c+i\omega\hat{E}_c-i(g_m-\beta f b)\hat{E}_s}{2(\alpha q S+1+S)} + a_{2,k}\frac{-R+\alpha S g_m+\alpha S^2\beta f q\tilde{E}_{2,\rm dc}}{\alpha(\alpha q S+1+S)}\\
&+ \alpha S^2\beta f q a_{2,k+1}\frac{\tilde{E}_{2,c}+i\tilde{E}_{2,s}}{2\alpha(\alpha q S+1+S)} + \alpha S^2\beta f q a_{2,k-1}\frac{\tilde{E}_{2,c}-i\tilde{E}_{2,s}}{2\alpha(\alpha q S+1+S)} + \alpha S^2\beta f q a_{2,k+2}\frac{\tilde{E}_{2,2c}+i\tilde{E}_{2,2s}}{2\alpha(\alpha q S+1+S)}\\
&+ \alpha S^2\beta f q a_{2,k-2}\frac{\tilde{E}_{2,2c}-i\tilde{E}_{2,2s}}{2\alpha(\alpha q S+1+S)} - a_{1,k}\left(\frac{\alpha S q+1+\alpha S g_m-\alpha S\beta f q\tilde{E}_{1,\rm dc}}{\alpha(\alpha q S+1+S)}+ik\omega\right)\\
&+ \alpha S\beta f q a_{1,k+1}\frac{\tilde{E}_{1,c}+i\tilde{E}_{1,s}}{2\alpha(\alpha q S+1+S)} + \alpha S\beta f q a_{1,k-1}\frac{\tilde{E}_{1,c}-i\tilde{E}_{1,s}}{2\alpha(\alpha q S+1+S)} + \alpha S\beta f q a_{1,k+2}\frac{\tilde{E}_{1,2c}+i\tilde{E}_{1,2s}}{2\alpha(\alpha q S+1+S)}\\
&+ \alpha S\beta f q a_{1,k-2}\frac{\tilde{E}_{1,2c}-i\tilde{E}_{1,2s}}{2\alpha(\alpha q S+1+S)}.\end{aligned} \tag{D14}$$

[1] K. Cole, *Membranes, Ions and Impulses* (University of California Press, Berkeley, 1968).
[2] B. Bean, Nat. Rev. Neurosci. **8**, 451 (2007).
[3] C. D. McCaig, A. M. Rajnicek, B. Song, and M. Zhao, Physiol. Rev. **85**, 943 (2005).
[4] C. D. McCaig, B. Song, and A. M. Rajnicek, J. Cell Sci. **122**, 4267 (2009).
[5] M. Zhao, Semin. Cell Dev. Biol. **20**, 674 (2009).
[6] M. A. Messerli and D. M. Graham, Biol. Bull. **221**, 7992 (2011).
[7] S. Chatkaew and M. Leonetti, Eur. Phys. J. E **17**, 203 (2005).
[8] P. A. Kralchevsky, T. D. Gurkov, and K. Nagayama, J. Colloid Interface Sci. **180**, 619 (1996).
[9] H. N. W. Lekkerkerker, Physica A **159**, 319 (1989).
[10] B. Duplantier, R. E. Goldstein, V. Romero-Rochin, and A. I. Pesci, Phys. Rev. Lett. **65**, 508 (1990).
[11] T. Chou, M. V. Jaric, and E. D. Siggia, Biophys. J. **72**, 2042 (1997).
[12] M. Winterhalter and W. Helfrich, J. Phys. Chem. **92**, 6865 (1988).
[13] Y. W. Kim and W. Sung, Europhys. Lett. **58**, 147 (2002).
[14] V. Kumaran, Phys. Rev. E **64**, 011911 (2001).
[15] V. Kumaran, Phys. Rev. E **64**, 051922 (2001).
[16] V. Kumaran, Phys. Rev. Lett. **85**, 4996 (2000).
[17] R. M. Thaokar and V. Kumaran, Phys. Rev. E **66**, 051913 (2002).
[18] P. Sens and H. Isambert, Phys. Rev. Lett. **88**, 128102 (2002).
[19] D. Lacoste, M. C. Lagomarsino, and J. F. Joanny, Europhys. Lett. **77**, 18006 (2007).
[20] T. Ambjornsson, M. A. Lomholt, and P. L. Hansen, Phys. Rev. E **75**, 051916 (2007).
[21] D. Lacoste, G. I. Menon, M. Z. Bazant, and J. F. Joanny, Eur. Phys. J. E **28**, 243 (2009).
[22] F. Ziebert, M. Z. Bazant, and D. Lacoste, Phys. Rev. E **81**, 031912 (2010).
[23] F. Ziebert and D. Lacoste, New J. Phys. **12**, 095002 (2010).
[24] J. T. Schwalbe, P. M. Vlahovska, and M. J. Miksis, Phys. Fluids **23**, 041701 (2011).
[25] J. Seiwert, M. J. Miksis, and P. M. Vlahovska, J. Fluid Mech. **706**, 58 (2012).
[26] P. M. Vlahovska, in *Advances in Planar Lipid Bilayers and Liposomes*, edited by A. Iglic (Elsevier, Amsterdam, 2010), Vol. 12, pp. 103–146.
[27] F. Ziebert and D. Lacoste, in *Advances in Planar Lipid Bilayers and Liposomes*, edited by A. Iglic (Elsevier, Amsterdam, 2011), Vol. 14, pp. 63–95.
[28] R. Dimova, K. A. Riske, S. Aranda, N. Bezlyepkina, R. L. Knorr, and R. Lipowsky, Soft Matter **3**, 817 (2007).
[29] R. Dimova, N. Bezlyepkina, M. D. Jordo, R. L. Knorr, K. A. Riske, M. Staykova, P. M. Vlahovska, T. Yamamoto, P. Yang, and R. Lipowsky, Soft Matter **5**, 3201 (2009).
[30] K. A. Riske and R. Dimova, Biophys. J. **91**, 1778 (2006).

[31] K. Riske, R. Knorr, and R. Dimova, Soft Matter **5**, 1983 (2009).
[32] K. A. Riske and R. Dimova, Biophys. J. **88**, 1143 (2005).
[33] R. L. Knorr, M. Staykova, R. S. Gracia, and R. Dimova, Soft Matter **6**, 1990 (2010).
[34] M. Staykova, R. Lipowsky, and R. Dimova, Soft Matter **4**, 2168 (2008).
[35] T. Charitat, S. Lecuyer, and G. Fragneto, Eur. Phys. J. E **21**, 153 (2006).
[36] S. A. Roberts and S. Kumar, J. Fluid Mech. **631**, 255 (2009).
[37] G. I. Taylor and A. D. McEwan, J. Fluid Mech. **22**, 1 (1965).
[38] J. R. Melcher and C. Smith, Phys. Fluids **12**, 778 (1969).
[39] P. Gambhire and R. M. Thaokar, Phys. Fluids **22**, 064103 (2010).
[40] W. Helfrich, Z. Naturforsch. **28c**, 693 (1973).
[41] U. Seifert, Eur. Phys. J. B **8**, 405 (1999).
[42] U. Seifert, Z. Phys. B **97**, 299 (1995).
[43] D. A. Saville, Annu. Rev. Fluid Mech. **29**, 27 (1997).
[44] J. C. Baygents and D. A. Saville, *Proceedings of the Third International Colloquium*, edited by T. Wang (AIP, New York, 1988), pp. 7–17.
[45] P. M. Vlahovska, R. S. Gracia, S. Aranda-Espinoza, and R. Dimova, Biophys. J. **96**, 4789 (2009).
[46] P. F. Salipante, R. Knorr, R. Dimova, and P. M. Vlahovska, Soft Matter **8**, 3810 (2012).
[47] J. R. Melcher and G. I. Taylor, Annu. Rev. Fluid Mech. **1**, 111 (1969).
[48] F. Brochard and J. F. Lennon, J. Phys. (France) **36**, 1035 (1975).
[49] J. Prost, J.-B. Manneville, and R. Bruinsma, Eur. Phys. J. B **1**, 465 (1997).
[50] C. A. Klausmeier, Theor. Ecol. **1**, 153 (2008).
[51] R. Grimshaw, *Nonlinear Ordinary Differential Equations* (CRC, Ann Arbor, 1993).
[52] M. Kummrow and W. Helfrich, Phys. Rev. A **44**, 8356 (1991).